Int. J. Solids Structures Vol. 27, No. 9, pp. 1085–1111, 1991
Printed in Great Britain.

0020–7683/91 $3.00+ .00

THE INITIATION AND PROPAGATION OF A LOCALIZED INSTABILITY IN AN INFLATED ELASTIC TUBE

STELIOS KYRIAKIDES and YU-CHUNG CHANG
Engineering Mechanics Research Laboratory, Department of Aerospace Engineering and Engineering Mechanics, The University of Texas at Austin, Austin, TX 78712, U.S.A.

(*Received* 20 *October* 1989; *in revised form* 28 *March* 1990)

Abstract—A thin elastic tube, when inflated, first expands to a cylindrical shape. After some deformation, this is interrupted by the development of a bulge somewhere along the length of the tube. For some rubber materials, the bulge initially grows with decreasing pressure, whereas the rest of the tube unloads. After growing to a certain diameter, the bulge starts spreading axially. This can occur at a well defined value of pressure which is much lower than the pressure required to initiate the bulge. The mechanisms through which the bulge is initiated, its initial growth and its eventual propagation along the length of the tube are studied experimentally and analytically. The results vividly illustrate localization and propagation types of instabilities which govern the mechanical behavior of a variety of solids and structures.

NOTATION

A	undeformed tube cross-sectional area
F	axial force
H, h	undeformed and deformed tube wall thicknesses
L, l	undeformed and deformed tube half lengths
P	pressure
P_I	bulge initiation pressure
P_P	bulge propagation pressure
R, r	undeformed and deformed radii
S, s	undeformed and deformed meridional coordinates
T_α	principal stress resultants
(u, w)	perturbation displacements
v, v_0	deformed and undeformed volumes enclosed by membrane
$W, \hat{W}$	strain energy density functions
w_0	radial imperfection amplitude
α_n	material constants
κ_α	membrane principal curvatures
λ	stretch ratio
λ_1	meridional stretch ratio
λ_2	azimuthal stretch ratio
λ_{2C}	λ_2 at bulge crown point
μ	rubber initial shear modulus
μ_n	material constants
σ	true stress
ω	angle $[\cos^{-1}(dz/ds)]$

INTRODUCTION

The inflation of a thin-walled, elastic, cylindrical tube is a problem which vividly illustrates the initiation of a localized instability and the mechanism through which this is transformed into an instability that propagates. As the tube is inflated, it first expands radially and axially in a uniform fashion. However, the extent to which the tube can grow uniformly is limited. The cylindrical configuration becomes unstable, and a local bulge appears somewhere along the length of the tube. The bulge initially grows while the pressure inside the tube drops. Because of the dropping pressure, the sections of the tube away from the bulge experience unloading. This type of behavior is known as localization (see Tvergaard and Needleman, 1980, for a broad discussion of structural problems with this behavior). If the pressure is prescribed, the longitudinal growth of the bulge is unstable. However, under volume control loading, the longitudinal growth can occur in a steady state fashion at a

well defined value of pressure. The pressure required to maintain quasi-static propagation of the bulge is known as propagation pressure (P_P). This pressure is usually much lower than that required to initiate the bulge (initiation pressure, P_I). The bulge continues to grow axially until the whole length of tube is inflated. Inflation beyond this point again results in cylindrical expansion of the tube, which occurs in a stable (increasing load) fashion.

An indication that this particular structure can be expected to have a rather complex behavior is obtained from the nature of the response calculated if the tube is limited to deform in a strictly cylindrical fashion. The pressure–volume response calculated with this restriction, for a particular latex rubber tube, is shown in Fig. 1a. The pressure sharply rises to a maximum (local) value; it then drops to a minimum (local) value, and it then gradually rises again. The circumferential true stress in the cylindrical membrane is proportional to the applied pressure P, to the square of the induced azimuthal stretch λ_2 and to the axial stretch λ_1. These, and the nature of the material stress–strain behavior shown in Fig. 1b, limit the maximum pressure that can be initially sustained by the tube (much like the area reduction and the relatively small modulus of many structural materials in the plastic range which limit the maximum load that can be applied to a bar under uniaxial tension). In a cylindrically deforming tube, the deformation and stress continue to grow monotonically after the pressure maximum, but with a decreasing pressure. At higher values of deformation, the material response stiffens again. Further increase in stress and deformation again requires higher pressure, resulting in the upturn observed in the pressure–volume response. If axial tension is applied simultaneously, the pressure required for inflation is lower but the other features of the response remain the same.

Chater and Hutchinson (1984) showed how the propagation pressure can be obtained from a simple, but exact, energy consideration of the steady state propagation process (Maxwell construction). The issue was further explored in a follow-up paper (see Kyriakides and Chang, 1990) by the present authors, in which the effect of axial load was also included. The propagation pressure predicted by this method for the example discussed is included in Fig. 1a.

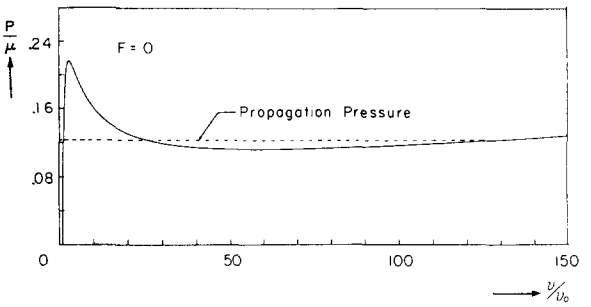

Fig. 1a. Pressure–volume response of cylindrically inflated latex rubber tube (P_p calculated by Maxwell construction).

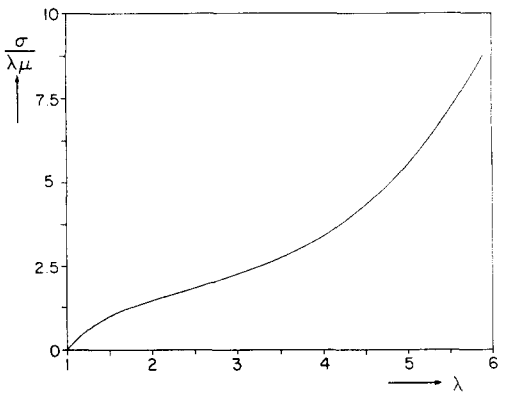

Fig. 1b. Uniaxial stress–deformation response of latex rubber.

The presence of a load maximum in the response indicates that an instability which can lead to localized deformation is possible. Indeed, it will be shown that the initiation and initial growth of the bulge is qualitatively similar to the initiation and initial growth of a neck in metal bars in tension (see Chen, 1971; Needleman, 1972). Of course, in the case of metals, the growth of the neck is interrupted due to fracturing.

The longitudinal spreading of the bulge and its development into a propagating instability is qualitatively similar to the phenomena of propagating buckles encountered in long metal cylindrical shell structures such as pipelines (see Palmer and Martin, 1975; Kyriakides and Babcock, 1981; Chater and Hutchinson, 1984; Kyriakides *et al.*, 1984) and tunnel liners (Kyriakides, 1986). The mechanisms of initiating and propagating necks in polymeric rods (and other geometries) are also qualitatively similar (G'Sell *et al.*, 1983; Hutchinson and Neale, 1983; Neale and Tugcu, 1985). Materials which undergo load-induced phase transformations have a similar phenomenological behavior (see Krishnan and Brown, 1973).

Because of the similarity of its mechanical behavior to those of the practical problems mentioned, and, in view of the relative simplicity of the experimental and analytical efforts required for its study, the problem of inflating a rubber tube is ideal as a model for demonstrating localization and propagation types of instabilities. This paper presents the results of combined experimental and analytical efforts which examine the mechanism through which an inflated and extended elastic tube first becomes unstable, how the bulge forms, and how it develops into a propagating instability.

EXPERIMENTS

A series of experiments were conducted in order to observe and record the onset of instability and the formation of a localized bulge during the inflation of elastic tubes. The experiments were conducted on commercially available natural rubber latex tubes. The tubes had a nominal outside diameter of 0.50 in. (12.7 mm), wall thickness of 0.063 in. (1.60 mm) and lengths that ranged between 5 and 36 tube diameters. The experimental set-up used is shown schematically in Fig. 2. One end of the tube was clamped to a rigid manifold while the other was sealed but left free. Axial load was applied by connecting the free end to a hanging, calibrated weight with a fine, flexible cable.

The tube and all accessories connected to it were filled with water, taking care to keep any trapped air (bubbles) to a minimum. The effect of the weight of the water inside the tube was negated by immersing the tube in water. This was achieved by placing the simple text fixture in a bath of water as shown in Fig. 2. The walls of the bath are transparent to allow observation of the experiment.

A positive displacement precision metering pump was used to inflate the tube. The pumping rate used delivered $0.062\, v_0\, s^{-1}$, where v_0 is the initial internal volume of each test

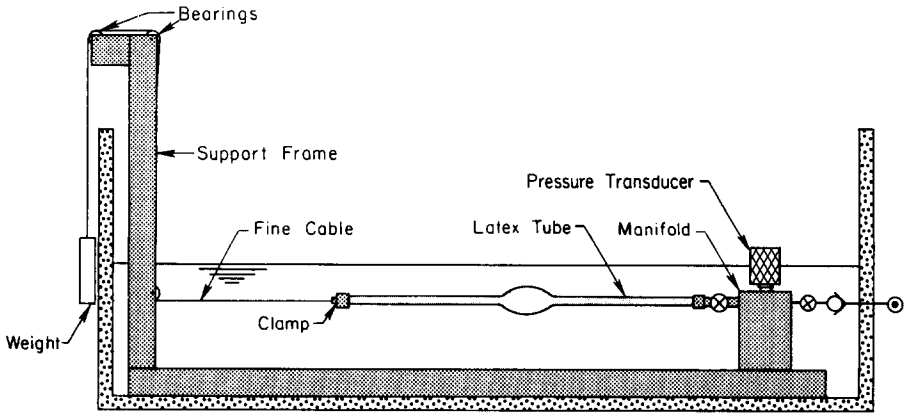

Fig. 2. Experimental set-up.

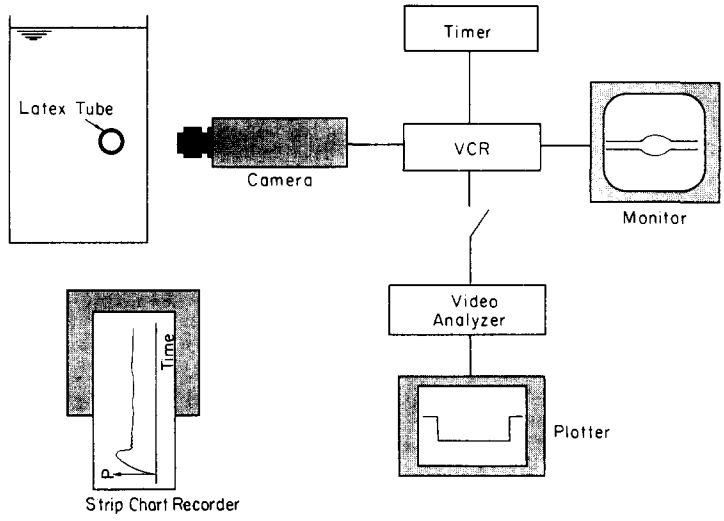

Fig. 3. Experiment monitoring and data acquisition systems.

specimen; i.e. as the length of the test specimens varied, the pump was adjusted to deliver approximately the same volume ratio per second. This was done in order to have some parity in loading rate (at least up to the onset of instability) between the different experiments. A one-way valve was used at the inlet of the manifold to reduce the possibility of backflow at all times. This water supply arrangement is considered to represent a good approximation of a volume control loading condition.

A high resolution video system was used to monitor and record the deformed configurations of the tube during inflation. Events were recorded at the rate of 30 frames s^{-1}. The pressure in the tube was monitored with a calibrated pressure transducer. The transducer output was recorded on a common time base with the video recording. The monitoring and recording set up used are shown in Fig. 3.

A video analyzer was used to obtain specific dimensional measurements from the recorded configuration history. These were matched with the corresponding pressure measurements. The pressure measurements had an uncertainty of 0.5% and the dimensional measurements had an uncertainty of 1%. The time base used had an uncertainty of approximately 3%.

Material properties

Independent experiments were conducted in order to measure properties of the latex tubes used in the inflation experiments. Details of the experimental procedure followed can be found in Kyriakides and Chang (1990). The results were used to obtain material constants for the strain energy density function suggested by Ogden (1972) and given by

$$W = \sum_{n=1}^{3} \mu_n(\lambda_1^{\alpha_n} + \lambda_2^{\alpha_n} + \lambda_3^{\alpha_n} - 3)/\alpha_n, \tag{1}$$

where λ_i are the principal stretches and α_n and μ_n are material constants. The material was assumed to be incompressible and the following values of α_n and μ_n were found to best fit the measured material responses:

$$\begin{aligned} \mu_1 &= 89.4 \text{ psi } (617 \text{ kPa}), & \alpha_1 &= 1.30, \\ \mu_2 &= 0.270 \text{ psi } (1.86 \text{ kPa}), & \alpha_2 &= 5.08, \\ \mu_3 &= -1.42 \text{ psi } (-9.79 \text{ kPa}), & \alpha_3 &= -2.00. \end{aligned} \tag{2}$$

The initial shear modulus of the material is given by

$$\mu = \tfrac{1}{2} \sum_{n=1}^{3} \mu_n \alpha_n = 60.4\,\text{psi}\,(416\,\text{kPa}). \tag{3}$$

Experimental results

A typical set of experimental results is shown in Fig. 4. The case shown involved a tube of length $L/R = 20.6$ (length of tube = $2L$, diameter = $2R$). A constant axial load of $F/\mu A = 0.383$ (A = initial cross-sectional area of tube) was applied during the inflation process. The initial part of the pressure–time history recorded and a sequence of tube configurations obtained from the video are shown in the figure. The pressure corresponding to each tube configuration is marked on the pressure–time recording. The following sequence of events was observed during the experiment: at the early stages of the inflation process the tube deformed essentially uniformly (except at the ends), growing both diametrically as well as axially. At first the pressure rose sharply with time but the rate of increase gradually decreased until a maximum value was reached. Very close to the pressure maximum, a localized bulge developed somewhere along the length of the tube. With the appearance of the bulge the pressure in the tube started to drop. The initial pressure drop was sudden (indicated by a dashed line in Fig. 4) but, eventually, the deformation process returned to a controlled quasi-static rate of growth. The sudden jump can be explained as follows. The downturn in pressure caused unloading in most of the tube except in the bulged section, which continued to grow monotonically. As a result of the unloading experienced by the cylindrical sections of the tube, the volume enclosed must be reduced. In the bulged region the enclosed volume increased. In the experiments, the volume of fluid inside the test specimen was prescribed. As a result, if the tube was short enough, so that the volume increase in the bulge was larger than the volume decrease in the cylindrical ends, the unloading could occur in a controlled fashion; i.e., without jumps in deformation (this is only possible for tubes with an initial length of a few diameters). If the tube was longer, so that the opposite was true, the initial unloading occurred dynamically as the structure "snapped" to a configuration which had the same internal volume. The longer the initial length of the tube, the greater the jump and the less controlled the deformation process. This issue will be further discussed with the help of the numerical results presented in later sections.

Continued pumping of water into the tube caused growth of the bulge, as shown in Fig. 4. At the same time, the pressure dropped gradually and asymptotically approached a steady state value. The bulge eventually stopped growing diametrically and started growing axially. During the axial spreading of the bulge, the shape of the transition between the inflated and "uninflated" sections was maintained and the pressure remained constant. This constant value of pressure is known as the bulge propagation pressure (see Chater and Hutchinson, 1984; Kyriakides and Chang, 1990). Configuration 10 in Fig. 4 is at this pressure.

Once this steady state condition was reached, the experiment was accelerated by increasing the pumping rate by a factor of 3. The bulge gradually spread over the whole length of the tube. Inflation beyond this point resulted in cylindrical expansion of the whole tube (i.e., diametrical and axial expansion) at increasing values of pressure. The experiment was usually terminated at this stage.

A series of similar experiments was conducted in which the length of the tube and the applied axial load were varied. Representative results obtained from these experiments are shown in Figs 5a and 6a. Figure 5a shows a set of measured pressure–radial stretch ratio (λ_{2C}) responses for four different tube lengths. In the experimental results, λ_{2C} is the stretch ratio of the outer surface of the tube at the crown-point of the bulge. The applied axial force was $F/\mu A = 0.383$. In each case, the part of the response which occurred dynamically is indicated with a dashed line, as the recorded pressure values are not dependable. The response for the shortest of the four tubes ($L/R = 6.86$) does not have a discontinuity for the reasons discussed above. In the other three responses, the discontinuity is seen to

increase with the tube length. We also observe that the response for the shortest tube is somewhat higher than the other three, which appear to be almost coincident.

Figure 6a shows a set of pressure–crown point stretch ratio responses for tubes which had a length of $L/R = 20.6$ for four different values of axial load F. The axial load reduces the value of the pressure maximum and similarly reduces the value of the propagation pressure as reported in Kyriakides and Chang (1990). In addition, the pressure drop at the discontinuity is seen to decrease with tension.

In order to investigate the effect of test specimen length on the initial postbuckling behavior of the tube (i.e., on the geometry of the bulge at its early stages), the profiles of bulges from tubes with lengths of $L/R = 6.86$, 13.7, 20.6 and 27.5 are compared in Fig. 7. The axial load applied in the four experiments was $F/\mu A = 1.148$. In addition, the bulge crown point has a radial stretch ratio of $\lambda_{2C} = 2.36$ for all cases. An image processing system consisting of a Grinnell 270 display system coupled with a VAX-IDL data processing system was used to reduce the video data. The "roughness" appearing on the surface of each bulge is due to resolution limitations of the recording and processing systems. Although the four profiles shown in Fig. 7 have some minor differences, their general dimensions and shapes are very similar. It seems that although the initiation of each bulge may depend on the length of the test specimen, the eventual bulge shape is independent of the specimen length. We also note that for longer tubes the bulge shape was found to be independent of the axial position at which it occurred.

The shape of the bulge was found to be significantly altered by axial load. This difference is illustrated in Fig. 8 where bulge profiles with the same crown point radial stretch ratios ($\lambda_{2C} = 2.36$) are shown for values of axial load of $F/\mu A = 0.383$, 0.766, 1.149 and 1.531. The four test specimens had a length of $L/R = 20.6$.

ANALYSIS

We consider an elastic, circular cylindrical membrane which has an initial radius R, wall thickness H and length $2L$. The cylinder is closed at the two ends with rigid plates of radius R. The closed tube is pressurized internally with a fluid pressure P which causes radial expansion and axial stretching. An additional external axial tensile load F is applied at the rigid closures. We limit our attention to deformations which are axisymmetric as well as symmetric about the cylinder mid-span. We adopt the coordinates (R, Z) and (r, z) for the undeformed and deformed configurations respectively, as shown in Fig. 9. In addition, S and s represent measures of length along the undeformed and deformed meridians respectively, and ω is the angle between the normal to the deformed membrane and the radial direction.

Membranes with small, axisymmetric deviations from the circular cylindrical shape will also be considered; thus, in general

$$R = R(Z). \tag{4}$$

The governing equations for finite deformations of axisymmetric membranes can be found in Green and Adkins (1960) and are summarized below. The deformed geometry is described by

$$\frac{dr}{ds} = \sin\omega, \quad \frac{dz}{ds} = -\cos\omega, \tag{5}$$

and the principal curvatures κ_1 and κ_2 are given by

$$\kappa_1 = -\frac{d\omega}{ds} \quad \text{and} \quad \kappa_2 = \frac{\cos\omega}{r}. \tag{6}$$

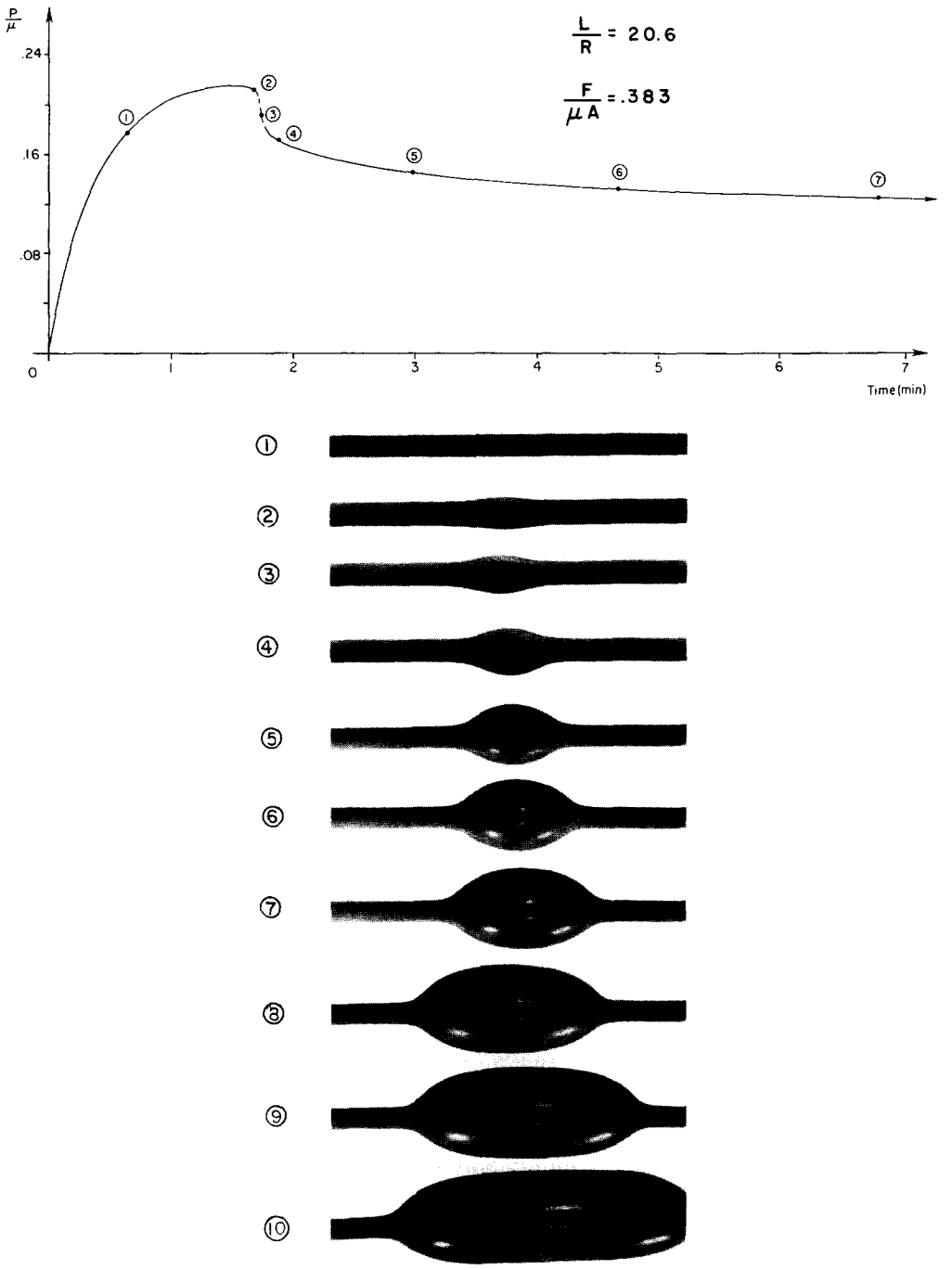

Fig. 4. Recorded pressure–time history and selected corresponding tube configurations.

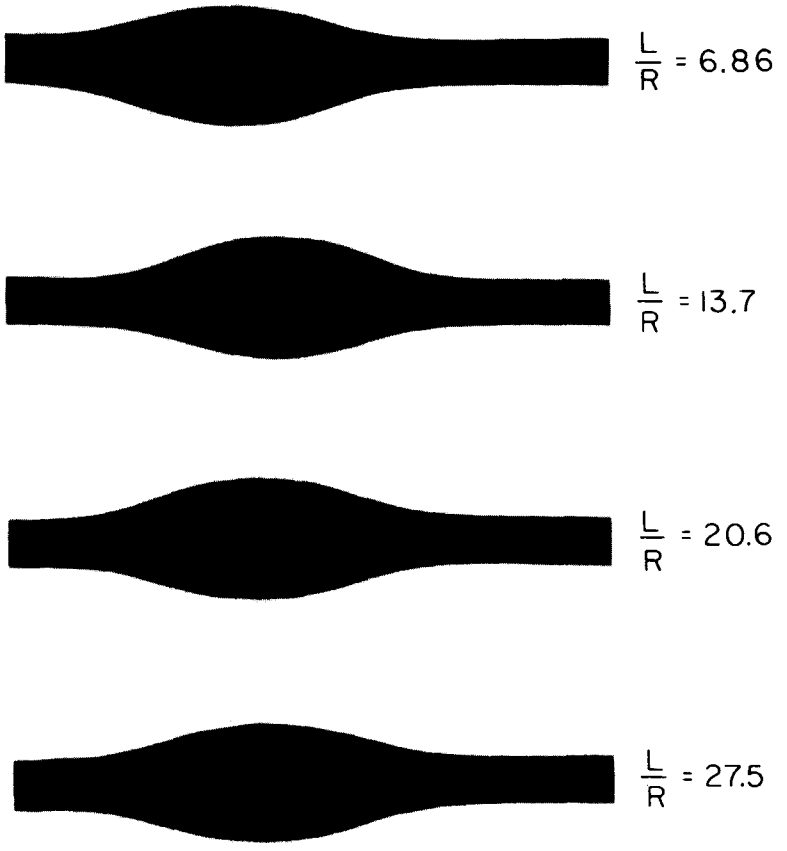

ig. 7. Comparison of bulges from tubes with different initial length ($F/\mu A = 1.148$, $\lambda_{2C} = 2.36$).

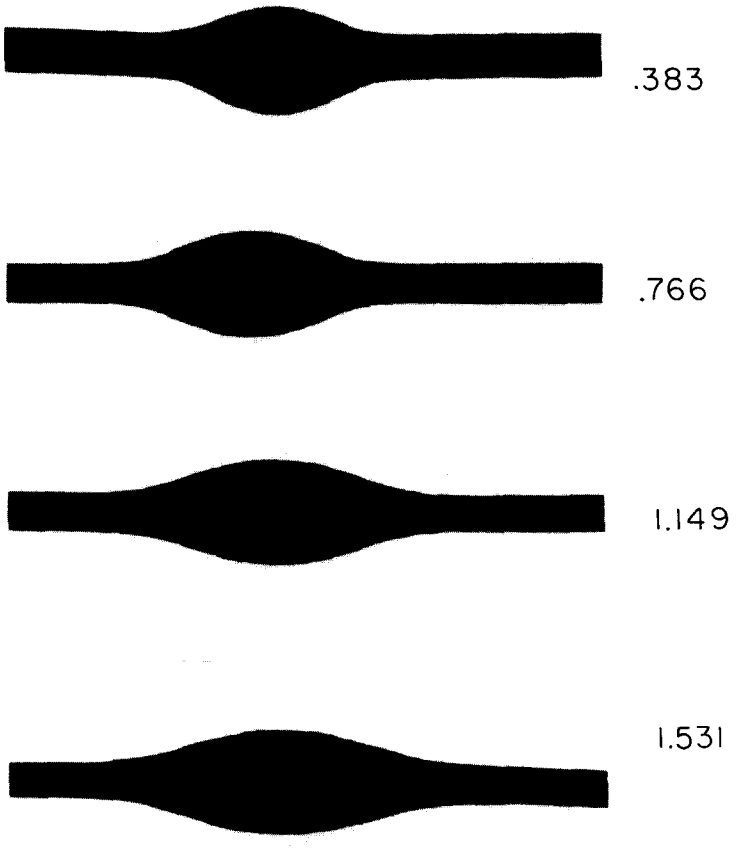

Fig. 8. Bulges with the same maximum radial stretch ratios from experiments with different axial loads.

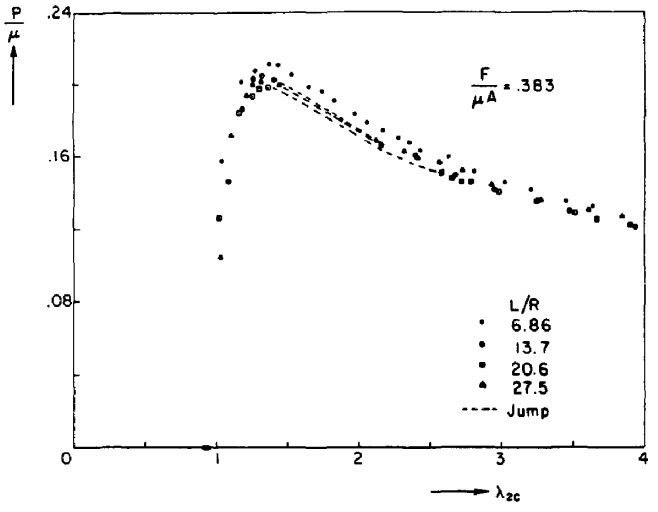

Fig. 5a. Experimental pressure–bulge crown point radial stretch ratio responses for tubes of various lengths.

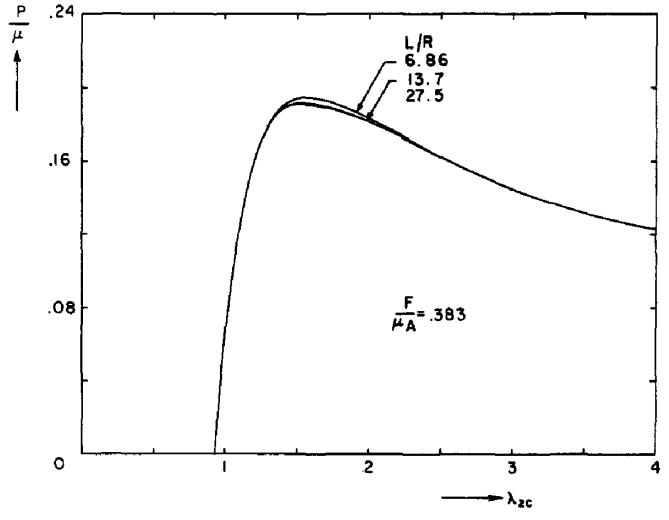

Fig. 5b. Predicted pressure–bulge crown point radial stretch ratio responses for tubes of various lengths.

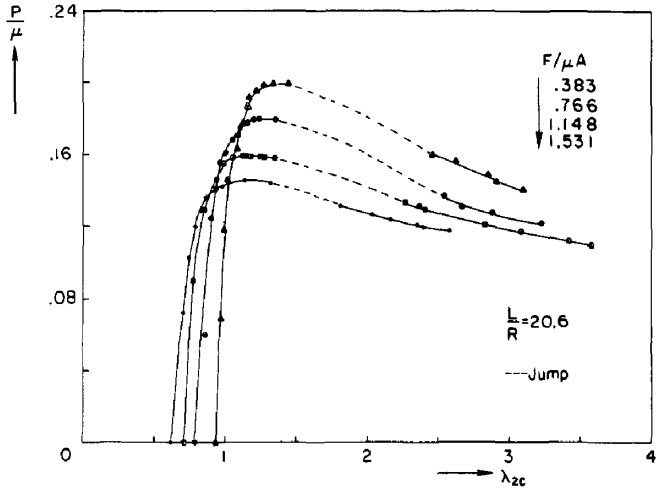

Fig. 6a. Experimental pressure–crown point radial stretch ratio responses of tubes at various axial loads.

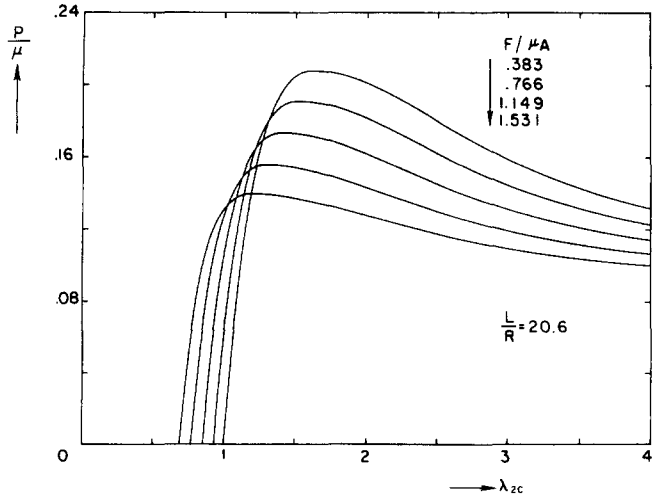

Fig. 6b. Predicted crown point–radial stretch ratio responses of tubes at various axial loads.

The principal stretches for incompressible membrane material are

$$\lambda_1 = \frac{ds}{dS}, \quad \lambda_2 = \frac{r}{R} \quad \text{and} \quad \lambda_3 = (\lambda_1\lambda_2)^{-1}. \tag{7}$$

We denote the stress resultants in the meridional and azimuthal directions by T_1 and T_2 respectively. The equilibrium equations can be expressed as follows:

$$2\pi R\lambda_2 T_1 \cos\omega = \pi R^2\lambda_2^2 P + F \tag{8a}$$

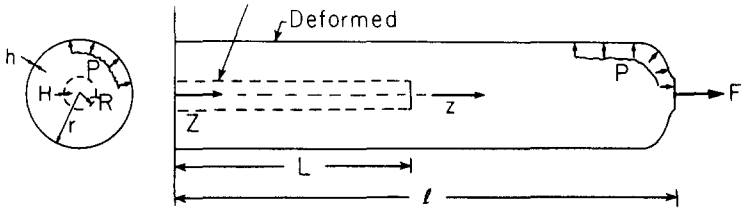

Fig. 9a. Cylindrical membrane geometry.

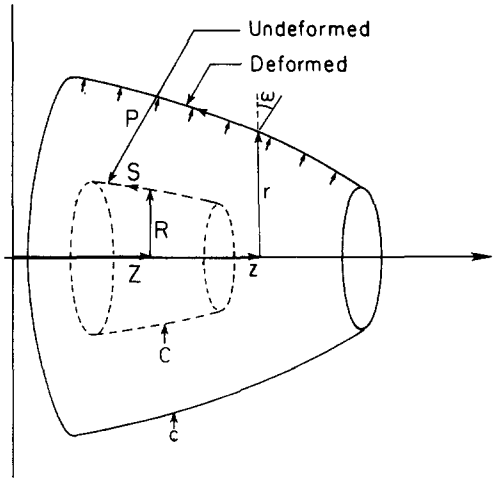

Fig. 9b. Axisymmetric membrane coordinates.

and

$$T_1\kappa_1 + T_2\kappa_2 = P. \tag{8b}$$

The material is assumed to possess a strain energy density function given by

$$\hat{W}(\lambda_1, \lambda_2) = W(\lambda_1, \lambda_2, (\lambda_1\lambda_2)^{-1}). \tag{9}$$

In the calculations that follow we adopt the form of $\hat{W}$ proposed by Ogden (1) with the constants measured experimentally (2). Using (9), the stress resultants can be related to the principal stretches as follows:

$$T_1 = \frac{H}{\lambda_2}\hat{W}_{,1}, \quad T_2 = \frac{H}{\lambda_1}\hat{W}_{,2}, \tag{10}$$

where $\hat{W}_{,\alpha} \equiv \partial\hat{W}/\partial\lambda_\alpha$.

Due to their complexity, eqns (5)–(10) must be solved numerically. It was found to be convenient to rearrange them into the following system of ordinary differential equations:

$$\begin{aligned}
\frac{d\lambda_1}{dZ} &= \frac{1}{R\hat{W}_{,11}}[(\lambda_2\hat{W}_{,12} - \hat{W}_{,1})R' + \sin\omega(\hat{W}_{,2} - \lambda_1\hat{W}_{,12})S'], \\
\frac{d\lambda_2}{dZ} &= \frac{1}{R}[\lambda_1 \sin\omega S' - \lambda_2 R'], \quad 0 \leqslant Z \leqslant L \\
\frac{d\omega}{dZ} &= \frac{1}{R\hat{W}_{,1}}\left[\cos\omega\left(\hat{W}_{,2} - 2\frac{\lambda_1}{\lambda_2}\hat{W}_{,1}\right) + \frac{F}{\pi RH}\frac{\lambda_1}{\lambda_2}\right]S', \\
\frac{dz}{dZ} &= -\lambda_1\cos\omega S',
\end{aligned} \tag{11}$$

where $R' \equiv dR/dZ$ and $S' \equiv dS/dZ$.

In developing these equations $dP/dZ = 0$ was used and the value of F is assumed to be prescribed. The boundary conditions appropriate for the problem are as follows:

$$\omega(0) = 0, \quad z(0) = 0, \quad \lambda_2(L) = 1 \quad \text{and} \quad \lambda_2(0) = \lambda_2^* \quad \text{or} \quad z(L) = l^*, \tag{12}$$

where λ_2^* and l^* are prescribed quantities. For every prescribed value of λ_2^* (or l^*), eqns (11) with boundary conditions (12) constitute a two-point boundary value problem which was solved numerically. The method adopted (developed by Pereyra, 1979) uses a finite difference scheme to discretize the problem domain, and Newton's method to solve the resultant set of nonlinear algebraic equations. For every converged solution $(\lambda_1(Z), \lambda_2(Z), \omega(Z), z(Z))$, $0 \leqslant Z \leqslant L$, the value of pressure required for equilibrium can be evaluated from (8a) using the values of the variables at any one of the difference points. The volume enclosed by the axisymmetric membrane can be found as follows:

$$v = \int_0^L -\pi R^2\lambda_2^2\lambda_1\cos\omega S'\,dZ. \tag{13}$$

During the initial stages of the loading, λ_2^* was prescribed incrementally. The tube initially grows in a nearly cylindrical fashion. After some deformation, a localized bulge forms at the mid-span of the cylinder. At first the bulge grows radially, until some value of $\lambda_2(0)$ is reached, and then starts to grow axially while its diameter remains unchanged. This continues until the whole length of the cylinder is inflated, as observed in the experiments. During this part of the loading history, the half length of the tube, l^*, was prescribed as it experiences monotonic growth (an alternative "loading" parameter to l^* is the volume v enclosed by the membrane).

Bifurcation analysis

The initial onset of instability of uniformly extended and inflated elastic tubes can be established by considering the linearized equilibrium equations of perturbations about the uniform state. The stability of circular cylindrical membranes has been extensively studied by Corneliussen and Shield (1961), Shield (1971, 1972), Haughton and Ogden (1979) and others, for a variety of loads and boundary conditions. Fourney and Stern (1968) examined the stability of the corresponding shell problem, whereas Haughton and Ogden (1979) considered the stability of similarly-loaded thick-walled elastic cylinders. Based on the results in the last two references, the influence of bending and other thick wall effects on the onset of instability is relatively small except in very thick tubes. We thus continue to treat the tube as a thin, elastic, incompressible membrane and directly adopt the method and formulation of Shield (1971, 1972).

We again consider a cylinder of initial radius R, wall thickness H and length $2L$. One end of the cylinder is fixed and the other is closed with a rigid, circular plate of radius R, which is free to move axially. The cylinder is inflated with an incompressible fluid in a volume control fashion. As before, a constant axial force F is applied at the free end. These loads cause uniform extension to a length $2\lambda_1 L$ and expansion to a radius of $\lambda_2 R$ (i.e. in the bifurcation analysis the effect of the boundary restraints is assumed to be negligible for long cylinders). The principal stress resultants can be obtained from (8) and are

$$T_1 = \frac{\lambda_2 RP}{2} + \frac{F}{2\pi R\lambda_2} \tag{14a}$$

and

$$T_2 = \lambda_2 RP. \tag{14b}$$

We consider the possibility of alternative, noncylindrical but axisymmetric equilibrium states by perturbing the inflated cylinder such that:

$$(\lambda_1 Z, \lambda_2 R) \to (\lambda_1 Z + u, \lambda_2 R + w)$$

where $u(Z)$, $w(Z)$ are displacement components representing the perturbation. Shield (1972) calculated the potential energy of the perturbed state to second order in u and w. Following his methodology it can be shown that the onset of instability occurs when the following functional has its minimum value:

$$Q = \pi RH \int_0^{2L} \left[(\alpha_1 - \alpha_6)\left(\frac{w}{R}\right)^2 + \alpha_2 u_{,Z}^2 + \alpha_7 w_{,Z}^2 + 2\alpha_8 u_{,Z}\left(\frac{w}{R}\right) \right] \mathrm{d}Z$$
$$+ \Lambda 2\pi\lambda_2 R \left[\int_0^{2L} \lambda_1 w \, \mathrm{d}Z + \frac{R\lambda_2}{2} u(2L) \right] \tag{15}$$

where Λ is a Lagrange multiplier. The values of α_i and some details on the results of (15) can be found in the Appendix.

PREDICTIONS AND DISCUSSION

Bifurcation instabilities

The bifurcation criterion (A3) was used to calculate the onset of instability of the tubes used in the experiment. The initial radius R of the cylindrical membrane was assumed to be equal to the mean radius of the actual tube used [i.e., $R = 0.2185$ in (5.55 mm)]. The main conclusion that can be drawn from the results of analysis is that instability first occurs after the pressure maximum. In spite of some differences in the material properties used in the calculations, this conclusion is congruent to those of Shield (1972) and Haughton and Ogden (1979).

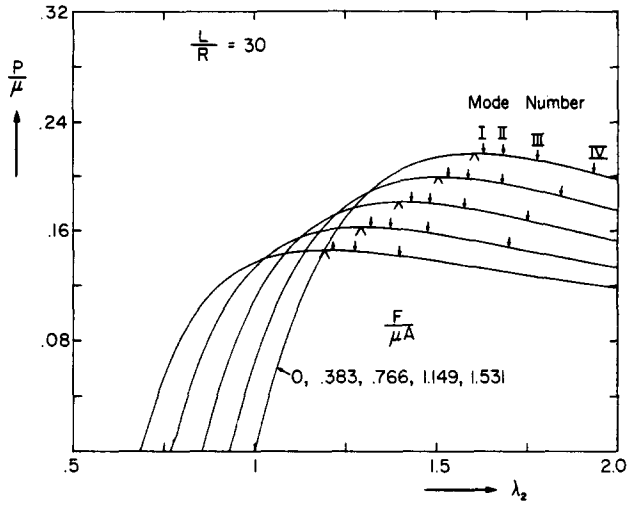

Fig. 10a. Trivial pressure–volume responses for various values of axial force and first four bifurcation points for $L/R \equiv 30$ (" $\wedge$ " $\equiv$ limit pressure, "$\downarrow$" $\equiv$ bifurcation point).

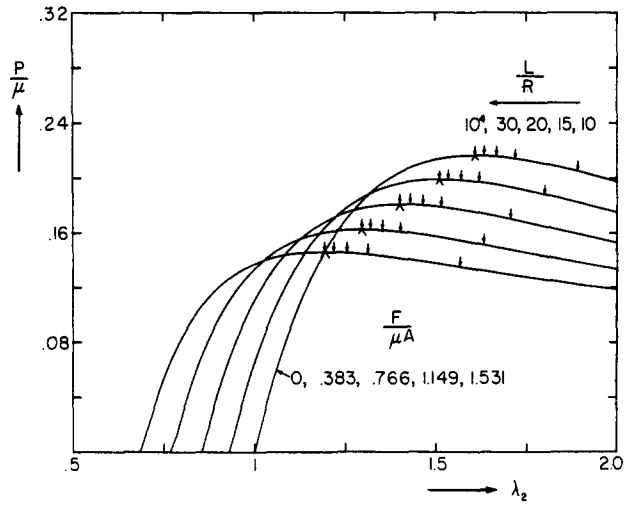

Fig. 10b. Trivial pressure–volume responses for various values of axial force and first bifurcation points for various tube lengths.

A sample of the results from the bifurcation analysis is shown in Fig. 10. Figure 10a shows the position of the first four bifurcation points on the trivial P–λ_2 responses, calculated for five values of prescribed axial loads. The tube analyzed had a length of $L/R = 30$. In each case, the first bifurcation point is seen to occur soon after the attainment of the pressure maximum (identified by " $\wedge$ "). Subsequent bifurcation points can be found, at progressively higher values of λ_2, by suppressing the existence of the preceding ones. The corresponding bifurcation modes are symmetric about the tube mid-span and have an increasing number of axial waves. This was found to be true for all values of axial load considered.

The initial length of the tube is an important geometric parameter affecting instability. Its effect is illustrated in Fig. 10b, which shows the position of the first bifurcation points for various tube lengths and the same values of prescribed axial load. For a very long tube ($L/R = 10^4$), the first bifurcation is almost coincident with the pressure maximum ($P/\mu = 0.2165$). This was found to be true for all values of tension considered. Reduction of the tube length delays the onset of instability to points downstream of the limit pressure. The length also affects the closeness of the bifurcation points. For a very long tube, many buckling modes are clustered together around the limit load. For shorter tubes, they occur

at increasingly greater λ_2 intervals. For example, a detailed analysis carried out for a tube of length $L/R = 10^4$ revealed that the λ_2 values at which the first and tenth bifurcation points occurred differed only in the sixth significant figure.

The closeness of the bifurcation modes may be one of the factors which leads to the initiation of bulges at almost any point along the length of the tube. Clearly, the presence of imperfections in the tubes used is another factor which influences the observed behavior.

The shape of the first bifurcation mode calculated for a tube of initial length $L/R = 15$ is sketched in Fig. 11a. The mode causes an expansion of the central part of the tube and a contraction at the ends. This mode shape is the same for tubes of all lengths. Thus, at least qualitatively, it can be seen that the tube bifurcates into a configuration which leads to accelerated deformation in the central part and reduction of deformation in other parts of the structure.

We conclude this section by observing that almost all the characteristics of the bifurcation instabilities mentioned have also been observed in analyses of instabilities leading to necking of bars in axial tension (see, for example, Hutchinson and Miles, 1974).

Localization/propagation of bulge

The method outlined in the analysis was used to calculate the deformation histories of tubes of various geometries. The major characteristics of the results are illustrated in Fig. 11. The tube analyzed had a length of $L/R = 15$. Motivated by the results from the bifurcation analysis, only axisymmetric deformations which are also symmetric about the tube mid-span were considered. An appropriate measure of the overall (mean) deformation of the structure is the volume enclosed by the deformed membrane. Figure 11a shows the

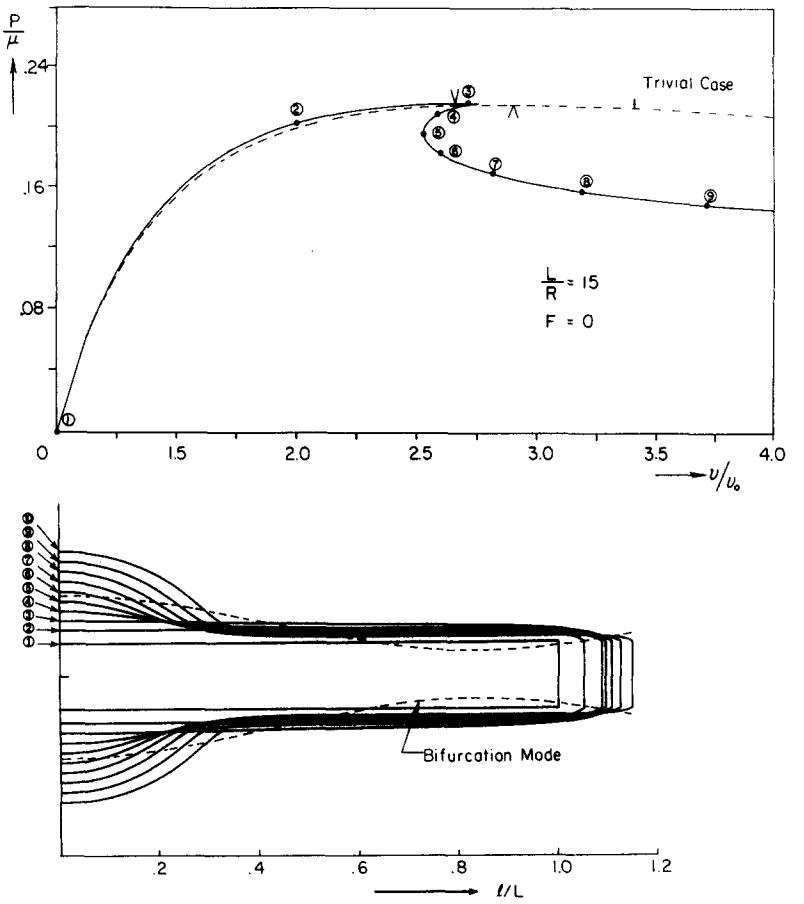

Fig. 11a. Calculated pressure–volume response and corresponding sequence of configurations during initiation of bulge.

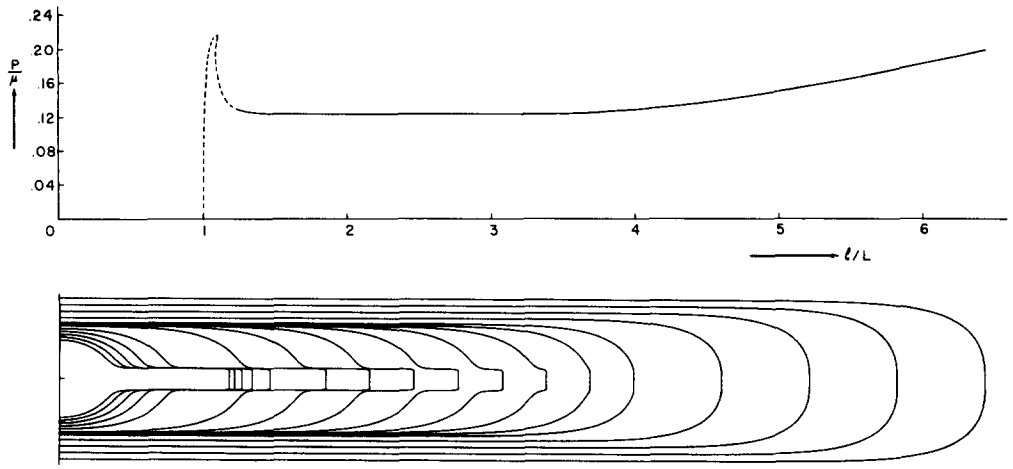

Fig. 11b. Pressure–deformed length response and sequence of configurations during propagation of bulge.

calculated pressure–volume response and the corresponding tube configurations during the early stages of the initiation of the bulge. Subsequent configurations and the corresponding pressure–deformed length responses are shown in Fig. 11b. Figure 12 shows a more complete pressure–volume response with the corresponding results from the trivially deformed tube.

Following Fig. 11a, we observe that the tube initially undergoes cylindrical deformations which are very close to the trivial solution. However, the radially fixed end condition at $Z = L$ causes a small, but finite, deviation from the cylindrical shape. The deviation takes the form of a very small, gradually varying curvature along the length of the tube. The end restraint results in a slightly higher response than the trivial one. In addition, the structure does not experience a sharp bifurcation of the type calculated in the previous section. The limit pressure on the actual response is marked in Fig. 11a with " $\vee$ ", and is seen to precede the limit pressure of the trivial solution (marked with " $\wedge$ "). Soon after the limit pressure, a sharp "cusp" develops in the P–v response. Some insight into the causes of this cusp can be gained by examining the corresponding local deformation (say λ_2) at $Z = 0$ and at $Z = 0.8L$.

The difference in deformation induced at the two points is very clearly illustrated in Fig. 13. Point A undergoes substantially less deformation than point C because of its proximity to the end constraint. When the limit pressure is reached and surpassed, the central section of the tube, which is already more deformed, experiences an accelerated radial growth. The ends never reach the maximum due to the end constraint. Thus, as the pressure starts to drop, they "unload". In summary, after the limit load, part of the structure experiences an increase in deformation and part of it a decrease. This is clearly seen in configurations 4–10 in Fig. 11a and is directly responsible for the initial appearance of the bulge.

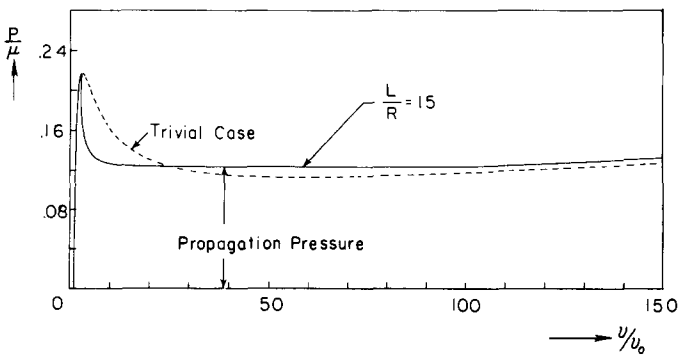

Fig. 12. Calculated pressure–volume response compared to that of cylindrical deformation.

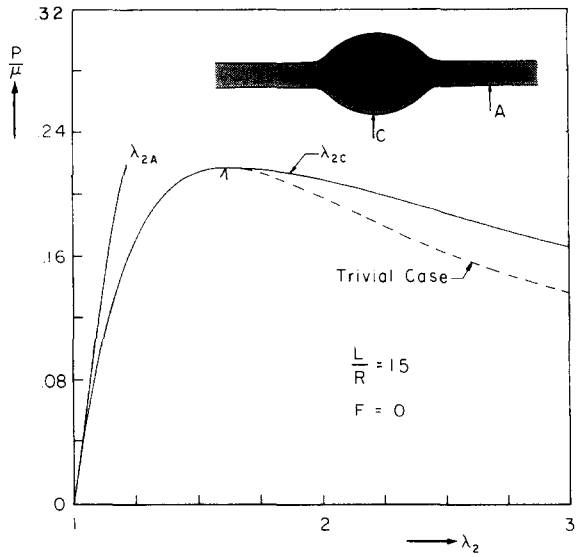

Fig. 13. Pressure–radial stretch ratio response at points A ($Z = 0.8L$) and C ($Z = 0.$).

Clearly, this sequence of events is not possible without the development of a load maximum. It would thus seem that a necessary condition for localization to occur is that the response has a limit load. This turn of events leads to a reduction in the enclosed volume in the cylindrical sections and an increase within the central part of the tube. In the particular case shown in the figure, the experienced decrease in volume is greater than the increase. As a result, the structure initially undergoes a net decrease in volume. This is the cause of the cusp observed in the P–v response. In a volume control experiment, a jump in pressure, bridging the cusp, would be experienced; this explains the behavior observed in the experiments reported earlier.

As the bulge grows, the volume required for continuing its growth becomes larger than the decrease in volume in the cylindrical ends. Thus, the net volume of the tube must be increased. Beyond the cusp, the volume increases monotonically while the pressure drops gradually. The bulge continutes to grow both axially and diametrically as shown in Fig. 11b. Eventually, it stops growing diametrically and starts spreading axially. This spreading occurs at a well-defined pressure plateau, and is stable if carried out under volume control. This continues until the whole length of the tube is inflated to the same diameter ($\lambda_2 \approx 5.6$). At the same time, the tube increases its length by approximately 4.1 times. This spreading of deformation at a constant level of load is very similar to the behavior observed in problems like those of propagating buckles, propagating necks and propagating phase boundaries as reported in the references given in the Introduction. Inflation beyond this point results in cylindrical deformations of the tube, as shown in Fig. 11b. This growth now requires an increase in pressure. Inflation can be continued until the material fails. The present analysis was carried out without regard to such material limitations.

The pressure–volume response for the complete analysis is shown in Fig. 12. The corresponding response for a cylindrically deformed tube is included for comparison. The latter can be viewed as the fundamental load–deformation response describing the structure, while the former is the actual response expected to be seen in a laboratory test of the structure.

For this particular case, the propagation pressure calculated from various types of analyses was as follows:

	P_P/μ
Complete membrane analysis	0.1229
Maxwell construction: membrane	0.1227
Maxwell construction: thick-walled tube	0.1262
Experiment	0.123

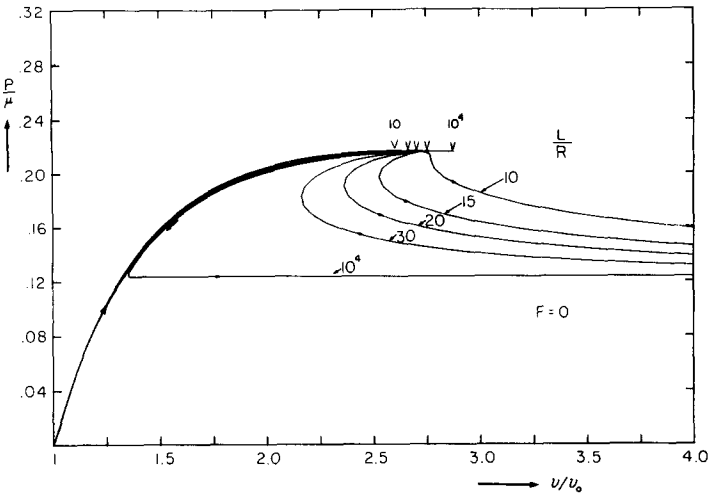

Fig. 14. Pressure–volume responses for tubes of different lengths.

Effect of tube length

The initial length of the tube was shown earlier to affect the bifurcation of the trivial solution. The effect of length on the stability of a tube with end restraints is illustrated in Fig. 14. The initial parts of the P–v responses of tubes with L/R of 10, 15, 20, 30 and 10^4 are shown. Initially the pressure and volume increase monotonically. The tube length has a relatively small effect on this part of the response for the range of values considered. However, the volume at which the maximum pressure is achieved (marked with " v ") and the size of the cusp that follows are significantly affected by L/R. The shortest of the five tubes analyzed develops a pressure maximum at the smallest value of v/v_0. Following the maximum, the response first experiences a very gradual decrease in pressure followed by a sudden pressure drop. The latter is associated with the initiation of the bulge. The delay between the maximum and the initiation of the bulge is similar to the delay seen earlier between the limit pressure and the bifurcation point for cylindrically deformed tubes of finite length. In this case, the development of the bulge proceeds with a monotonic increase in v. The tube length is such that the increase in volume in the bulged section is larger than the decrease in volume experienced elsewhere.

As the length of the tube increases, the limit load occurs at a larger value of volume. At the same time, the delay between the maximum and the instability is reduced (much like the results from the bifurcation analysis). For $L/R \geqslant 15$ a cusp develops in the response following the onset of instability. The size of the cusp grows with L/R for the reasons already given.

A very long tube ($L/R = 10^4$) was analyzed in the following approximate fashion. The inflation of a tube with $L/R = 50$ was numerically analyzed in the fashion described. A representative section, away from the two ends of the tube ($Z = 0.6L$), was used to obtain the local P–v response. This section was chosen because it was found to undergo cylindrical deformations. The volume change of this representative sample was multiplied by an appropriate constant factor. This was chosen to correspond to adding a uniformly deforming section at that point to increase the initial length to $L/R = 10^4$. This approach enabled us to calculate the response shown in Fig. 14. The limit load coincides with that calculated for the trivial case. The instability is seen to occur at the limit load, much in agreement with the results of the bifurcation analysis. Initially the volume increase experienced in the bulged section is relatively small. Most of the tube unloads and, as a result, the unloading follows *nearly* the same P–v path as the loading. More significantly, the pressure stops dropping when the value of the propagation pressure is reached.

In an experiment conducted under volume control on a tube of such length, the pressure can be expected to suddenly drop from P_L to P_P. The change will occur dynamically as the tube jumps from the cylindrical configuration to one which has a bulge of radius $r = \lambda_2^* R$

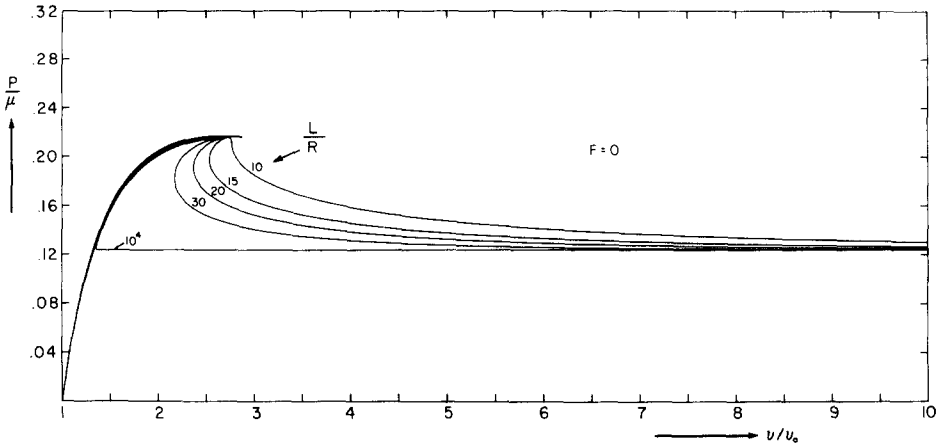

Fig. 15. Pressure–volume responses for tubes of different lengths.

and of a certain length. The length of the bulge will be such that it accommodates all the volume reduction caused by unloading the cylindrical part of the structure from P_L to P_P.

This illustrates that for long tubes the initial growth of the bulge is very difficult to control by prescribing a global deformation parameter (the volume in this case). (Complicated control schemes which are based on measurements local to the bulge can be considered.) Thus, we conclude that controlled initiation of the bulge under prescribed volume is only possible for short test specimens.

The position of the bulge along the length of the tube is almost arbitrary. In practice the bulge can be expected to occur in the section with the biggest initial imperfections (thickness, shape, material).

In spite of differences in the bulge initiation mechanism, the pressure asymptotically drops to the tube propagation pressure for all tube lengths considered. This is demonstrated in the results presented in Fig. 15. However, for tubes with shorter lengths the minimum pressure in the response may be higher than P_P.

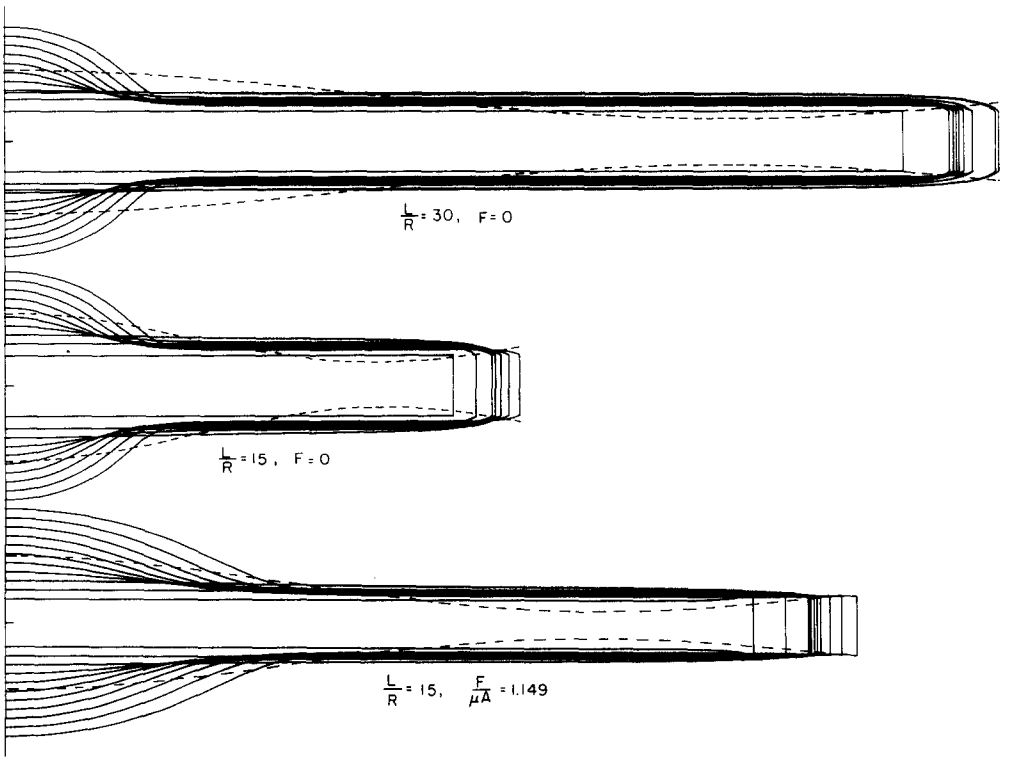

Fig. 16. Initial configurations of bulges in tubes of different lengths and axial loads.

Figure 16 shows the initial configurations of the bulging tubes for lengths of $L/R = 15$ and 30. No visible difference in the bulge shapes of the two tubes was detected. This was found to be true for all tube lengths analyzed. This result confirms the observations on the subject made from the experimental results presented in Fig. 7.

On the other hand, the length of the first bifurcation mode from the corresponding cylindrically deformed tube geometry is directly proportional to the tube length. Thus, the position of the node is, in both cases, approximately at $Z = 0.5L$ as can be seen in Fig. 16. It can thus be concluded that the bifurcation mode is the initial cause of nonuniform deformation, but the shape of the bulge which results from the bifurcation is governed by equilibrium considerations in the vicinity of the bulge. At the same time we repeat that the sequence of events that would be seen in an experiment is very much influenced by the length of the test specimen and the way the experiment is controlled.

Figure 17 shows pressure–deformation histories for tubes with $L/R = 30$. These correspond to the results shown in Fig. 13 for a shorter tube. For the longer tube, the effect of the end restraint is limited to a region close to the end of the tube. As a result, most of

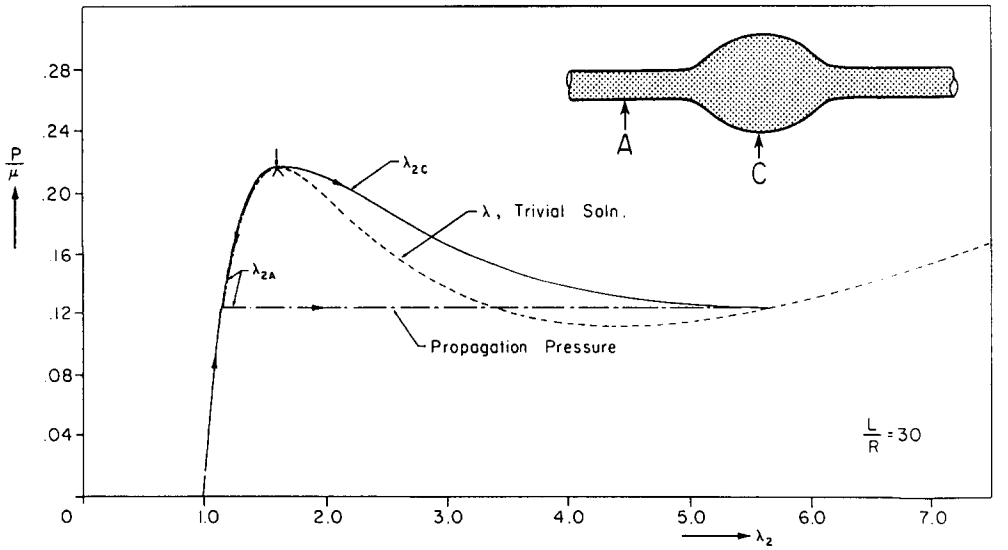

Fig. 17a. Comparison of calculated λ_2 values at two points along the tube length for $L/R = 30$.

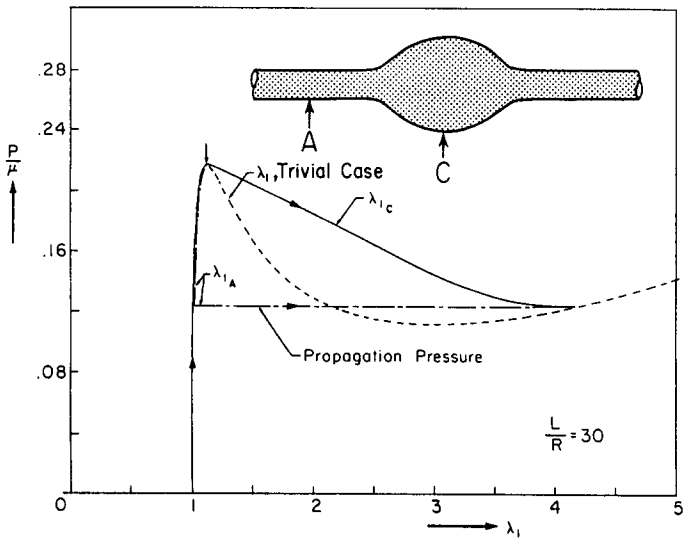

Fig. 17b. Comparison of calculated λ_1 values at two points along the tube length for $L/R = 30$.

the tube initially undergoes cylindrical deformations as shown in the figure. After the limit load is reached, the deformation in the bulged section grows, whereas the cylindrical sections experience reduction in deformation. The "bifurcation" into these two types of behavior occurs very close to the pressure maximum, as illustrated in the figure.

The general type of mechanism described above is similar to that governing necking instabilities which occur in tension tests on ductile materials (e.g., metals, polymers). The pressure–volume response in the current problems corresponds to the load–end displacement response in the tensile test. The P–λ_{2C} response corresponds to the load–λ_{2C} response in the necked region. The similarity can be confirmed by comparing the results in Figs 8 and 9 of the paper by Chen (1971) to those in Fig. 14 (for $L/R = 10$) and Fig. 13 of this paper respectively.

The effect of specimen length on the response does not seem to have been considered for the necking problems (probably due to the large computational time required). Based on the insight developed from this study we suggest that in a uniaxial test a very long metal bar can be expected to break on reaching the load maximum, even if loaded in displacement control. Unloading in metals is elastic and, as a result, the deformation recovered is only a small fraction of the deformation induced during loading. However, if the bar is long enough, the deformation recovered (shortening) from the sections away from the neck, undergoing unloading, can be larger than the increase in deformation (elongation) in the necked region. Thus, the load–displacement response of the bar will be very similar to the initial part of the P–v responses in Fig. 14. [The initial part of a cusp in the load–end displacement response was reported by Tvergaard *et al.* (1981) for a plane strain tensile test of a nonlinearly elastic material.]† A sudden drop in load can be expected, followed, most probably, by failure. For some polymeric materials, such as high density polyethylene, the neck will form and propagate much like the bulge described above (see G'Sell *et al.*, 1983). The specimen length can be expected to have a similar effect on the neck initiation process as in our problem. The magnitude of the effect will, however, be less pronounced due to the elastic–plastic nature of polyethylene.

It is interesting to ask whether the shape of the necked region for elastic–plastic materials is equally insensitive to the specimen length as the problem analyzed here.

Effect of tension

Axial tension has the effect of lowering the pressure required to inflate the tube. The pressure maximum and minimum in the trivial response occur at lower values (see Fig. 7 in Kyriakides and Chang, 1990). The actual response is similarly affected by tension. Figure 18 shows a set of responses corresponding to tubes of various lengths, all of which were inflated in the presence of an axial load of $F/\mu A = 1.149$. All features of the responses are the same as those of the case with $F = 0$, discussed in Fig. 14. The limit pressure (trivial case) for this case is $P_L/\mu = 0.1626$ and the propagation pressure $P_P/\mu = 0.1052$. The corresponding values for $F = 0$ were $P_L/\mu = 0.2165$ and $P_P/\mu = 0.1229$.

Figure 19 shows a set of calculated P–v responses for a tube of length $L/R = 27.5$ for various values of axial tension. The results confirm the characteristics described above. It is interesting to observe that the size of the cusp in these responses is reduced as the tensile force is increased.

As mentioned in the experimental section, the shape of the bulge is substantially altered by tension. A set of bulge configurations calculated for a tube of length $L/R = 15$ inflated in the presence of an axial load $F/\mu A = 1.149$ is shown in Fig. 15 together with those from the case with no tension. The difference in the two sets of profiles is quite clear from the figures.

Figure 20 shows a comparison of the bulge profiles at $\lambda_{2C} = 2.70$ for four different values of axial force. This comparison corresponds to the one presented earlier in Fig. 7 from experimental results. The predictions are in good agreement with the experiments. The profile of propagating bulges is also affected by tension. The presence of tension reduces

† Pointed out by V. Tvergaard.

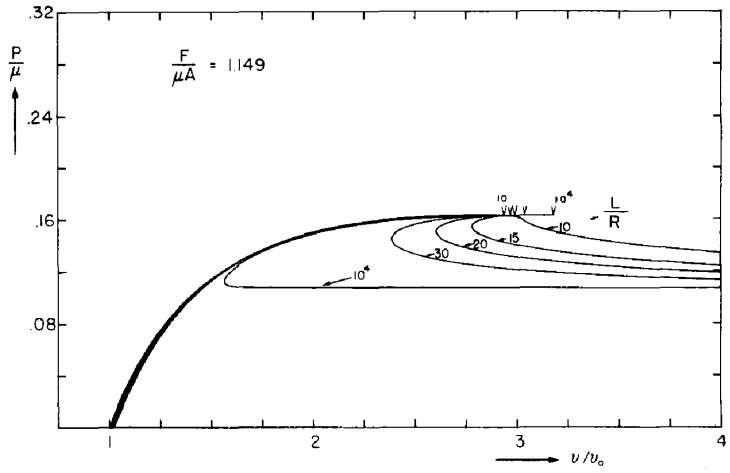

Fig. 18. Pressure–volume responses of tube with various lengths with $F/\mu A = 1.149$.

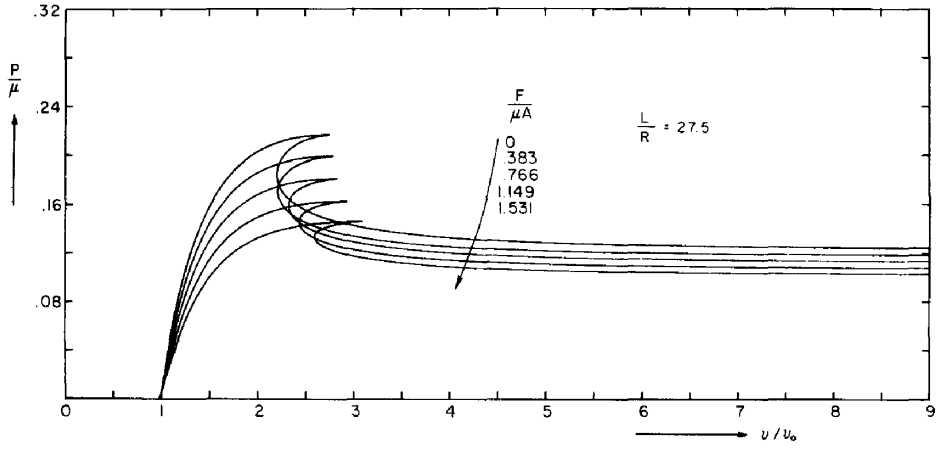

Fig. 19. Pressure–volume responses of tube at various values of axial force.

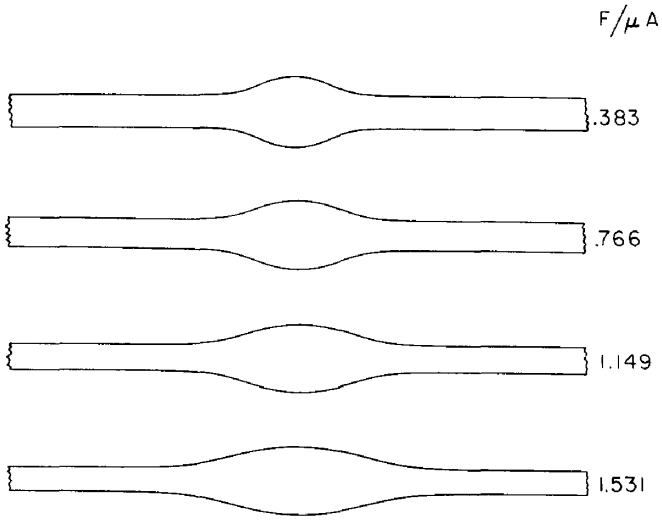

Fig. 20. Calculated bulge configurations at $\lambda_{2C} = 2.70$ for different values of axial force.

the diameter of a propagating bulge and increases the length of the transition region as demonstrated in Figs 13, 15 and 16 of Kyriakides and Chang (1990).

The experimental P–λ_{2C} responses presented in Fig. 6a were reproduced numerically and the results are shown in Fig. 6b. Again, the comparison between experiment and analysis is quite good.

Effect of imperfections

The manufacturing process can induce small deviations in wall thickness, and in the diameter of the tube. In addition, the material properties can vary along the length of the tube (this can result from improper initial preparation of the rubber, for example). The consequences of such imperfections were analyzed by considering the variation of these quantities to be axisymmetric. Figures 21 and 22 show a sample of the imperfection sensitivity study in which the tube radius was assumed to vary as follows:

$$R(Z) = R\left[1 + \frac{w_0(Z)}{R}\right]. \tag{16}$$

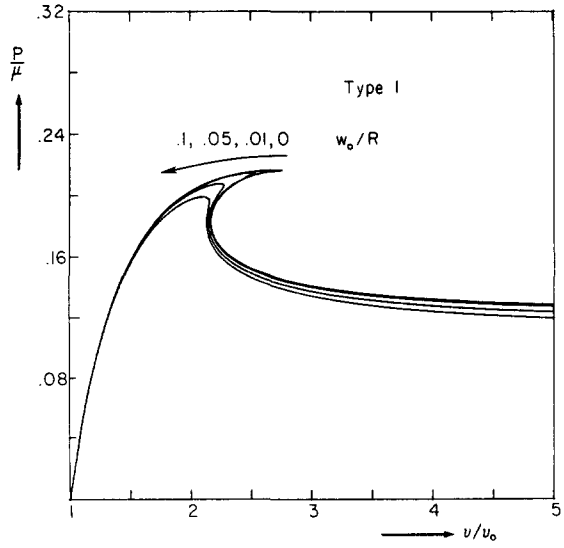

Fig. 21. Pressure–volume responses for various imperfection (type I) amplitudes.

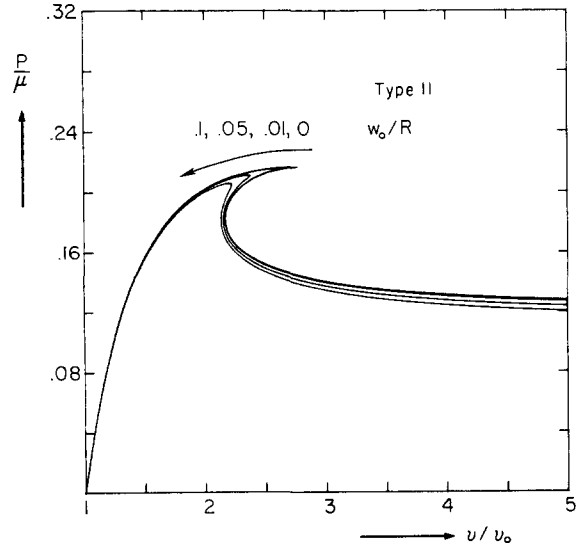

Fig. 22. Pressure–volume responses for various imperfection (type II) amplitudes.

Two different forms of $w_0(Z)$ were considered as follows:

Type I

$$w_0(Z) = w_0(\cos 2kL - 1)\sin kZ + \sin 2kL(1 - \cos kZ)] \tag{17}$$

where k is the first eigenvalue of the trivial problem calculated from (A3);

Type II

$$w_0(Z) = w_0\, e^{-\beta(Z/L)^2} \quad (\beta = 3 \ln 10) \tag{18}$$

which is commonly used for problems experiencing localization (e.g., Chen, 1971; Tvergaard and Needleman, 1980).

Figure 21 shows P–v responses for tubes of length $L/R = 30$ with imperfections of Type I and various amplitudes (w_0/R). In general, the effect of the imperfection on the limit pressure is small. Figure 22 shows similar results for Type II imperfections. The conclusions are the same. Similar results were obtained for imperfections in wall thickness and in material properties with the axial distribution as given in (17) and (18).

Thus, we conclude that, although imperfections will, in general, influence the position of localization, they do not cause significant reduction in the maximum load of the structure. The propagation pressure is equally unaffected by imperfections. Similar insensitivity to initial imperfections was observed in necking instabilities.

The effect of material properties

In order to demonstrate the effect of material properties on the bulge instability the material constants in the Ogden strain energy density function (1) were varied as follows:

$$W = \sum_{n=1}^{2} \frac{\mu_n}{\alpha_n}(\lambda_1^{\alpha_n} + \lambda_2^{\alpha_n} + (\lambda_1\lambda_2)^{-\alpha_n} - 3),$$

$$\mu = \tfrac{1}{2}(\mu_1\alpha_1 + \mu_2\alpha_2) = 60.4 \text{ psi (416 kPa)},$$

$$\mu_1 = 89.4 \text{ psi (617 kPa)}, \quad \alpha_1 = 1.30. \tag{19}$$

μ_2 was varied between 0.57 and 1.42 psi and α_2 was calculated from the second equation in (19). The geometry of the tube was kept the same as before.

The nominal stress–axial stretch relationships obtained for five different values of μ_2 are shown in Fig. 23. For the parameters used $\mu_2 = 1.42$ psi is approximately the largest value for which the uniaxial stress–stretch response is monotonically increasing. The nomi-

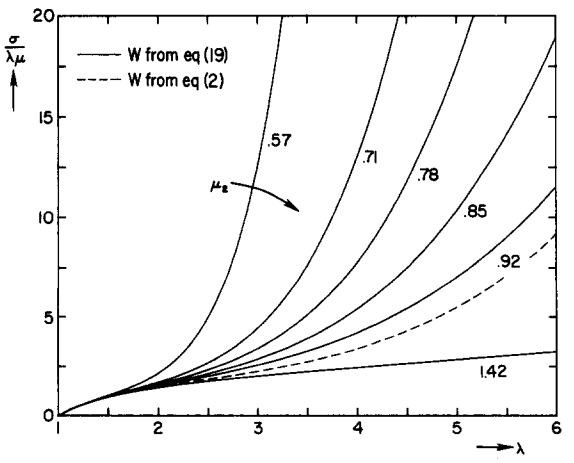

Fig. 23. Nominal stress–stretch relations obtained for different values of μ_2 in eqn (19).

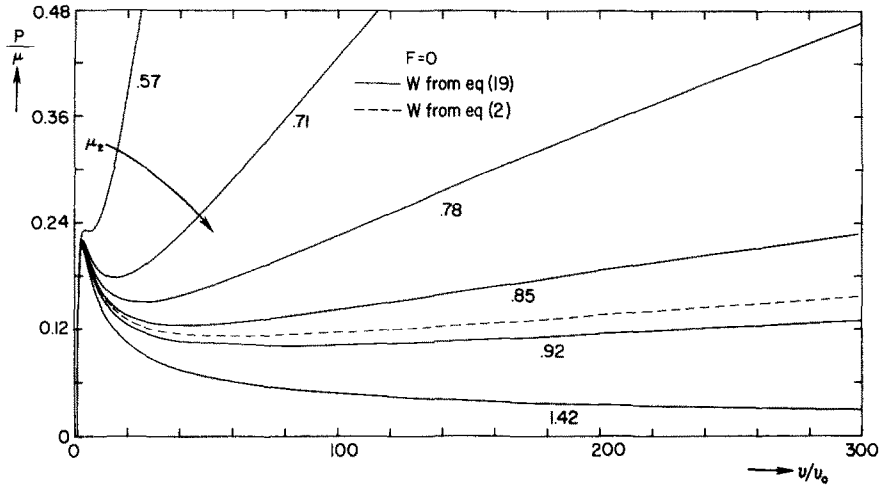

Fig. 24. Pressure–volume responses for cylindrical inflation of long tubes with different strain energy density functions.

nal stress–axial stretch relationship derived from the experimental measurements [eqns (1) and (2)] is shown with a dashed line in the same figure.

Each set of these material properties was used to calculate the pressure–volume response for cylindrical inflation of long tubes (trivial response). The results are shown in Fig. 24. For $\mu_2 = 0.57$ psi the pressure–volume response has a relatively small jump in volume at $P \simeq 0.23\mu$ but otherwise the pressure increases monotonically with volume. For $\mu_2 = 0.71$, 0.78, 0.85 and 0.92 psi the response has a distinct limit load followed by a drop to a local pressure minimum. The response grows monotonically after the pressure minimum. The value of the pressure minimum and the slope of the response after it decrease as μ_2 increases. For $\mu_2 = 1.42$ psi the pressure monotonically decreases after the pressure maximum.

Clearly we can expect that for $\mu_2 = 0.71$–0.92 psi the tube will develop a propagating instability. The propagation pressures predicted from the Maxwell construction for the different values of μ_2 are given in Fig. 25.

The material properties given in (19) were used in the axisymmetric membrane analysis in order to illustrate the effect of the material properties on the localization and propagation instabilities that occur. The tube analyzed was closed at both ends and had a length of $L/R = 15$ and $F = 0$. The pressure–length responses calculated for each value of μ_2 are shown in Fig. 26. For $\mu_2 = 0.57$ psi the pressure rises to a value of approximately $P \simeq 0.23\mu$

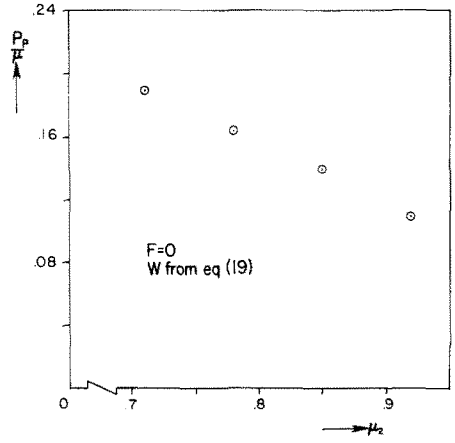

Fig. 25. Propagation pressures for different values of μ_2 in eqn (19) (Maxwell construction).

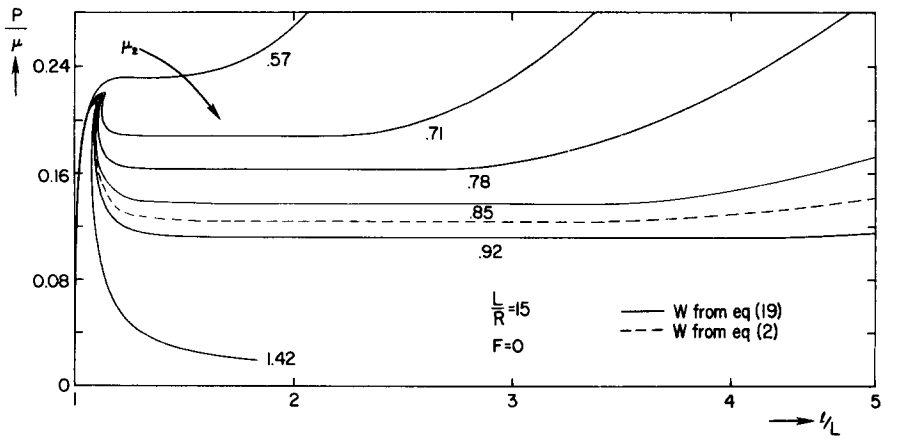

Fig. 26. Calculated pressure–deformed length responses for different values of μ_2.

and remains relatively constant until the length increases to approximately $1.6L$. Following this, the pressure increases monotonically with length. The structure does not experience localization. The tube deforms in a cylindrical fashion, as shown in Fig. 27. A similar behavior can be expected for values of $\mu_2 < 0.57$ psi. For $\mu_2 = 0.71$, 0.78, 0.85 and 0.92 psi the pressure–length response is characterized by a pressure maximum followed by a drop to a pressure plateau. The value of the pressure plateau decreases as μ_2 increases. In these cases a bulge is initiated at the pressure maximum. The bulge propagates along the length of the tube while the pressure remains constant. The axial deformation induced by the propagating bulge increases as the value of μ_2 increases. The shape of the propagating bulge profile also varies with μ_2. This can be seen by comparing the configurations calculated for $\mu_2 = 0.71$ psi in Fig. 27 with those presented in Fig. 11b.

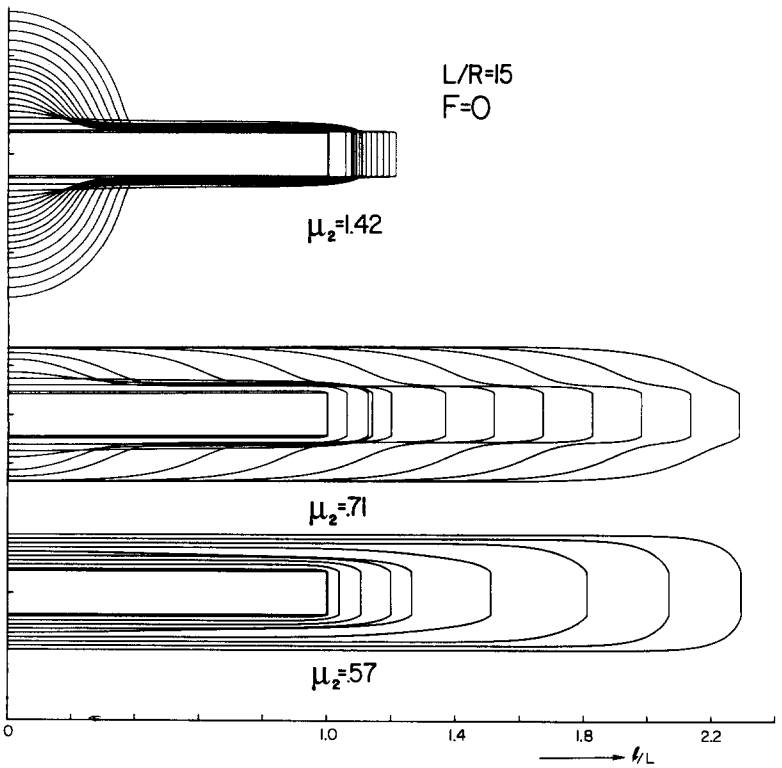

Fig. 27. Calculated configuration sequences of inflated tubes with different strain energy density functions [W as in eqn (19)].

For $\mu_2 = 1.42$ psi (and larger values) the tube experiences localization. At $P \approx 0.214\mu_2$ a bulge develops and starts growing. However, in this case the pressure monotonically decreases with deformation and as a result the bulge never propagates. The bulge is seen to grow in a nearly radial fashion in the sequence of configurations shown in Fig. 27.

Acknowledgement—The work reported was supported in part by the National Science Foundation through the PYI award MSM-8352370.

REFERENCES

Chater, E. and Hutchinson, J. W. (1984). On the propagation of bulges and buckles. *ASME J. Appl. Mech.* **51,** 269–277.

Chen, H. W. (1971). Necking of a bar. *Int. J. Solids Structures* **7,** 685–717.

Corneliussen, A. H. and Shield, R. T. (1961). Finite deformation of elastic membranes with application to the stability of an inflated and extended tube. *Arch. Rational Mech. Anal.* **7,** 273–304.

Fourney, W. F. and Stern, M. (1968). Stability of a finitely deformed thin cylindrical shell. *Int. J. Engng Sci.* **6,** 661–683.

Green, A. E. and Adkins, J. E. (1960). *Large Elastic Deformations and Non-Linear Continuum Mechanics*, Ch. 4. Oxford University Press, Oxford.

G'Sell, C., Ali-Helal, N. A. and Jonas, J. J. (1983). Effect of stress triaxiality of neck propagation during the tensile stretching of solid polymers. *J. Mater. Sci.* **18,** 1731–1742.

Haughton, D. M. and Ogden, R. W. (1979). Bifurcation of inflated circular cylinders of elastic material under axial loading, Parts I and II. *J. Mech. Phys. Solids* **27,** 179–212 and 489–512.

Hutchinson, J. W. and Miles, J. P. (1974). Bifurcation analysis of the onset of necking in an elastic/plastic cylinder under axial tension. *J. Mech. Phys. Solids* **22,** 61–71.

Hutchinson, J. W. and Neale, K. W. (1983). Neck propagation. *J. Mech. Phys. Solids* **31,** 405–426.

Krishnan, R. V. and Brown, L. C. (1973). Pseudoelasticity and the strain-memory effect in Ag-45 at % Cd alloy. *Metall. Trans.* **4,** 423–429.

Kyriakides, S. (1986). Propagating buckles in long confined cylindrical shells. *Int. J. Solids Structures* **22,** 1579–1597.

Kyriakides, S. and Babcock, C. D. (1981). Experimental determination of the propagation pressure of circular pipes. *ASME J. Press. Vess. Technol.* **103,** 328–336.

Kyriakides, S. and Chang, Y.-C. (1990). On the inflation of a long elastic tube in the presence of axial load. *Int. J. Solids Structures.* Babcock Memorial Volume **26,** 975–991.

Kyriakides, S., Yeh, M. K. and Roach, D. (1984). On the determination of the propagation pressure of long circular tubes. *ASME J. Press. Vess. Technol.* **106,** 151–159.

Neale, K. W. and Tugcu, P. (1985). Analysis of necking and neck propagation in polymeric materials. *J. Mech. Phys. Solids* **33,** 323–337.

Needleman, A. (1972). A numerical study of necking in circular cylindrical bars. *J. Mech. Phys. Solids* **20,** 111–127.

Ogden, R. W. (1972). Large deformation isotropic elasticity—on the correlation of theory and experiment for incompressible rubber-like solids. *Proc. R. Soc. Lond.* **A326,** 565–584.

Palmer, A. C. and Martin, J. H. (1975). Buckle propagation in submarine pipelines. *Nature* **254**(5495), 46–48.

Pereyra, V. (1979). PASVAC3: an adaptive finite difference Fortran program for first order nonlinear, ordinary boundary problems. In *Lecture Notes in Computer Science* (Edited by Goos and Hartmanis), Vol. 76, pp. 67–88. Springer, Berlin.

Shield, R. T. (1971). On the stability of finitely deformed elastic membranes; Part I: stability of a uniformly deformed plane membrane. *J. Appl. Math. Physics (ZAMP)* **22,** 1016–1028.

Shield, R. T. (1972). Part II: stability of inflated cylindrical and spherical membranes. *J. Appl. Math. Phys. (ZAMP)* **23,** 16–34.

Tvergaard, V. and Needleman, A. (1980). On the localization of buckling patterns. *ASME J. Appl. Mech.* **47,** 613–619.

Tvergaard, V., Needleman, A. and Lo, K. K. (1981). Flow localization in the plane strain tensile test. *J. Mech. Phys. Solids* **29,** 115–142.

APPENDIX

The material constants α_i in (15) have the following values:

$$\alpha_1 = \hat{W}_{22},$$
$$\alpha_2 = \hat{W}_{11},$$
$$\alpha_4 = \hat{W}_{12},$$
$$\alpha_6 = \frac{\hat{W}_2}{\lambda_2},$$
$$\alpha_7 = \frac{\hat{W}_1}{\lambda_1},$$
$$\alpha_8 = \alpha_4 - \frac{\lambda_2}{\lambda_1}\alpha_6, \tag{A1}$$

all evaluated at specific values of λ_1 and λ_2 which satisfy (14). The second term on the right-hand side of (15) is

a constraint requiring that the volume enclosed by the tube is not changed by the applied perturbation. The onset of instability is given by the nontrivial solution of the Euler differential equations of Q solved with the appropriate boundary conditions. These can be shown to be as follows:

$$\alpha_7 w_{,ZZ} - \alpha_8 \frac{u_{,Z}}{R} - (\alpha_1 - \alpha_6)\frac{w}{R^2} - \Lambda_1 = 0,$$

$$\alpha_2 u_{,ZZ} + \alpha_8 \frac{w_{,Z}}{R} = 0, \tag{A2}$$

with

$$w(0) = 0, \quad u(0) = 0, \quad w(2L) = 0$$

and

$$\int_0^{2L} \frac{w}{R}\,dZ + \frac{1}{2}\frac{\lambda_2}{\lambda_1}u(2L) = 0.$$

The eigenvalues are obtained by solving the following equation

$$\tan kL = (kL)\Gamma$$

where

$$k^2 = [\alpha_8^2 - (\alpha_1 - \alpha_2)\alpha_6]/R^2\alpha_2\alpha_7 \tag{A3}$$

and

$$\Gamma = \left\{1 - \frac{[\alpha_8^2 - (\alpha_1 - \alpha_2)\alpha_6]}{\left[2\alpha_2\left(\frac{\lambda_1}{\lambda_2}\right) - \alpha_8\right]^2}\right\}.$$

Thus a sequence of distinct eigenvalues exists very much in accordance with more conventional stability problems in structural mechanics. The bifurcation mode is given by

$$w = C[(\cos 2kL - 1)\sin kZ + \sin 2kL(1 - \cos kZ)]. \tag{A4}$$

$u(Z)$ can be evaluated from (A2) and (A4).